Carbohydrate Polymers 88 (2012) 1227–1232

Contents lists available at SciVerse ScienceDirect

Carbohydrate Polymers

journal homepage: www.elsevier.com/locate/carbpol

Synthesis of polysucrose-based nanoparticles by a one-step method

Wei Jiang[a,b], Hongying Jia[a,b], Zhe Zhang[a,b], Tiantian Gan[a,b], Xin Hou[a,b,*]

[a] School of Material Science and Engineering, Tianjin University, Tianjin 300072, PR China
[b] Tianjin Key Laboratory of Composite and Functional Materials, Tianjin 300072, PR China

ARTICLE INFO

Article history:
Received 9 December 2011
Received in revised form 11 January 2012
Accepted 29 January 2012
Available online 6 February 2012

Keywords:
Polysucrose
Nanoparticles
Self-assembling
Protein adsorption

ABSTRACT

A set of novel water-soluble polysucrose-based nanoparticles were prepared by a one-step self-assembly method using soluble polysucrose (PS) and acrylic acid (AA) as materials, ceric ammonium nitrate (CAN) as initiator and methylene-bisacrylamide (MBA) as crosslinker. Fourier transform infrared spectroscopy, ^{13}C nuclear magnetic resonance and scanning electron microscopy were utilized to characterize the structure and morphology. The results indicated the dimensions of the nanoparticles increased from 209.7 nm to 293 nm, and the polydispersity index (PDI) decreased, with the increase of AA content from 6.61 to 29.20 mmol/g, while the content of PS (2.5 g), the other components (R_{MI} = 220 and R_{MC} = 35) and experimental conditions were kept constant. The dimensions of nanoparticles increased from 244 nm to 281 nm and the PDI increased with the increase of initiator content from 0.04 to 0.12 mmol/g, while the content of AA (2.1 g), the other components (R_{SM} = 0.25 and R_{MC} = 35) and experimental conditions were kept constant.

1. Introduction

In recent years, polymeric nanoparticles have gained a great deal of attention in medical and biological fields due to the good performance of these nanoparticles, such as low toxicity, good biocompatibility and biodegradability. Meanwhile, the nanometer-sized carrier has advantage of site-specific drug targeting and extension of the circulation time (Gregory, Elias, & Patrick, 2001; Jae et al., 2000; Rodrigues et al., 2003). Polysucrose (PS) is a water-soluble polysaccharide with low toxicity, hydrophilicity, good biodegradability and biocompatibility. Its raw material, sucrose, is a renewable material with low prices and high purity, so it has wide applications in biomedical, pharmaceutical, and other related fields (Fischer, Waitz, Vollath, & Simha, 2008; Hari & Aruna, 2007; Suphiya & Sanjeeb, 2008).

At present PS, whose trade names include Ficoll400 and Dormacoll, have been widely used as density gradient agents for cell separation and as therapeutic agents (Donald, Annette, & Thomas, 1975; Peter, Olgal, & Olga, 1987; Richard, Andreas, & Wolfgang, 1986). However, we know of no report about using PS to prepare nanoparticles, though PS has a broad application prospect.

Self-assembling is an important preparation method for water phase nanoparticles. Traditional self-assembly methods for forming nanoparticles have utilized hydrophilic–hydrophobic balance of amphiphilic blocks or graft polymer in water medium. This method must use organic solvents as co-solvents and the synthesis of amphiphilic block or graft copolymer is required in the early stage of the preparation. At the same time, the nanoparticles prepared by traditional self-assembly method have a low concentration (<5 mg/ml) (Birringer, Gleiter, Klein, & Marquardt, 1984), and the efficiency is unsatisfactory. Thus a new preparing method for water phase nanoparticles with a higher efficiency would be highly useful.

In this paper, PS-based nanoparticles were prepared by hydrogen bond-driven self-assembly under appropriate conditions. This method can prepare nanoparticles efficiently in the water phase without organic solvents. Bovine serum albumin (BSA) was used as the adsorbate model to examine the adsorption behavior of the PS-based nanoparticles under different solution pH values.

2. Experimental

2.1. Materials

Polysucrose (PS, M_W = 400,000), which is soluble in water, was purchased from Polymer Science & Commerce Co., Ltd. (Tianjin, China). Ceric ammonium nitrate (CAN) was purchased from Tianjin Chemical Engineering Stock Co. (Jiangsu Province, China). Acrylic acid (AA) and methylene-bisacrylamide (MBA) were purchased from Tianjin No. 1 Chemical Reagent Plant (Tianjin, China). Sodium hydroxide (NaOH) and nitric acid (HNO_3) were obtained from

* Corresponding author at: School of Material Science and Engineering, Tianjin University, Tianjin 300072, PR China. Tel.: +86 022 27402346.
E-mail address: houxin@tju.edu.cn (X. Hou).

0144-8617/$ – see front matter © 2012 Elsevier Ltd. All rights reserved.
doi:10.1016/j.carbpol.2012.01.084

Table 1
The composition and yield of nanoparticles calculated from the weight-calculated approach (R_{MC} = 35).

Sample no.	$n_{SU\ (sucrose\ unit)}$:n_{AA} (R_{SM}) mol:mol	n_{AA}:$n_{Initiator}$ (R_{MI}) mol:mol	Yield (%)
S1	0.1	220	74.2
S2	0.15	220	73.8
S3	0.25	220	73.0
S4	0.35	220	71.8
S5	0.45	220	71.4
M1	0.25	103	77.2
M2	0.25	117	76.9
M3	0.25	137	76.3
M4	0.25	164	75.1
M5	0.25	220	70.1
M6	0.25	274	68.3

Samples S1–S5 were prepared with increasing gradually R_{SM} from 0.10 to 0.45 (i.e. reduced AA contents) and the R_{MI} and R_{MC} kept constant (R_{MI} = 220 and R_{MC} = 35). Samples M1–M6 were prepared while the R_{MI} was increased gradually from 103 to 247 (i.e. reduced initiator contents), and the R_{SM} and R_{MC} were kept constant (R_{SM} = 0.25 and R_{MC} = 35). The yield and composition of the nanoparticles were calculated by Eqs. (4)–(6). The results are shown in the table.

Tianjin Kewei Co. (Tianjin, China). All the chemical regents were analytical pure grade and used without further purification.

2.2. Preparation of PS-based nanoparticles

For all samples, 50 ml of 50 g/l (2.5 g) PS solution was added to a 250 ml three-necked flask at a water temperature of 40 °C. A selected amount of CAN was dissolved in 1.25 ml of 0.1 M of nitric acid solution and then added to the three-necked flask. After 4 min, a selected amount of AA was added and 30 min later a selected amount of MBA was introduced into the mixture. The reaction was continued for 7 h under the protection of nitrogen. At the end of the reaction, the pH value of the mixture was adjusted to neutral by aqueous NaOH solution (1 M). Finally, the reaction solution was dropped into a dialysis bag, and then dialyzed in deionized water for 72 h in order to removal unreacted monomer. The solution obtained by dialysis was lyophilized by freeze drying and then the solid nanoparticles obtained.

R_{MI} is defined as the molar-ratio of AA monomer and initiator CAN; R_{MC} is the molar-ratio of AA monomer and crosslinker MBA; R_{SM} is the molar-ratio of sucrose units and AA monomer.

Samples S1, S2, S3, S4 and S5 were prepared with increasing R_{SM} from 0.10 to 0.45 (i.e. reduced AA contents from 5.3 g to 1.2 g), while the content of PS was held constant, and the R_{MI} and R_{MC} kept constant (R_{MI} = 220 and R_{MC} = 35).

Samples M1, M2, M3, M4, M5 and M6 were prepared while the R_{MI} was decreased from 247 to 103 (i.e. increased initiator contents from 0.06 g to 0.16 g), and the R_{SM} and R_{MC} were kept constant (R_{SM} = 0.25 and R_{MC} = 35). Samples C1, C2, C3, C4, C5, C6, C7 and C8 were prepared while R_{MC} was decreased from 112 to 25 (i.e. increased crosslinker contents) and the R_{SM} and R_{MI} were kept constant (R_{MI} = 220 and R_{SM} = 0.25) (Table 1).

2.3. Characterization of polysucrose-based nanoparticles

2.3.1. Fourier transform infrared spectra

The Fourier transform infrared (FTIR) spectra were obtained using a Bio-Rad FTS 135 FTIR instrument (Bio-Rad, USA); the dried samples were powdered and mixed with KBr and then pressed into pellets under reduced pressure.

2.3.2. The morphology of PS-based nanoparticles

The product particles in aqueous solution were negatively stained by 5% of phosphotungstic acid, then dropped onto the copper mesh coated by a carbon film and dried for 72 h at room temperature. A transmission electron microscope (Philips CM 120 BioTwin, Netherlands) was used to characterize the PS-based nanoparticles structure.

2.3.3. The particle size and size distribution of PS-based nanoparticles

Water as dispersion medium, the particle sizes and the size distribution of the PS-based nanoparticles were determined using a Mastersizer S particle size analyzer (Malvern Instrument, UK). The polydispersity index (PDI) of PS-based nanoparticles was calculated according to:

$$\overline{D_n} = \frac{\sum_{i=1}^{n} d_i}{n} \quad (1)$$

$$\overline{D_w} = \frac{\sum_{i=1}^{n} d_i^4}{\sum_{i=1}^{n} d_i^3} \quad (2)$$

$$\mathrm{PDI} = \frac{\overline{D_w}}{\overline{D_n}} \quad (3)$$

where $\overline{D_n}$ represents the number average diameter calculated according to Eq. (1), $\overline{D_w}$ represents the weight average diameter calculated according to Eq. (2), and d_i means the diameter of the nanoparticles and n is the total number of the nanoparticles.

2.3.4. The yield of the product particles and composition

$$\mathrm{Yield} = \frac{W_S}{W_T} \times 100\% \quad (4)$$

$$C_{ps} = \frac{W_D}{W_S} \times 100\% \quad (5)$$

$$C_{IC} = \left(1 - \frac{W_D}{W_S}\right) \times 100\% \quad (6)$$

The yield of the product particles and composition were calculated according to the above equation, where W_S is the weight of solid nanoparticles after freeze drying; W_T is the total weight of all reactants; W_D is the weight of added PS; C_{PS} and C_{IC} are the percentage of PS and polyacrylic acid (PAA, including crosslinker), respectively.

2.4. Protein adsorption

Bovine serum albumin (BSA) was used as model protein to test the adsorption behavior of the porous PS microspheres. 0.01 mol/L Tris–HCl buffer solution was used to adjust the pH value of the BSA solution. The PS-based solution prepared was kept in a centrifuge for 0.5 h at a rotation rate of 4000 rpm, and then collect supernatant solutions. After the supernatant solutions being lyophilized by freeze drying, a white powder solid was obtained. Typically, the above dried nanoparticles (40 mg) were added to a BSA solution (5.0 ml, 2.5 mg/ml) with different pH (pH = 3.5, 6.0, 8.5) for 10 h in a shaking incubator (150 rpm) at 37 °C and then were maintained for 24 h at room temperature. Finally centrifugal separation was carried out for 2 h at a rotation rate of 16,000 rpm. After centrifugation, the optical density at 280 nm of the supernatant solutions was recorded, and the protein adsorbing efficiency and the amount of protein adsorbed were calculated by the following equation:

$$q = (C_0 - C_1) \times V \quad (7)$$

$$\mathrm{AE} = \frac{q}{W_S} \times 100\% \quad (8)$$

Here q represents the amount of protein adsorbed; AE is the protein adsorbing efficiency of the nanoparticles; C_0 is the concentration of BSA in the liquid phase before adsorption (mg/ml); C_1 is the concentration of BSA in the liquid phase after adsorption (mg/ml); V is the volume of solvent (ml) and W_S is the mass of nanoparticles (g).

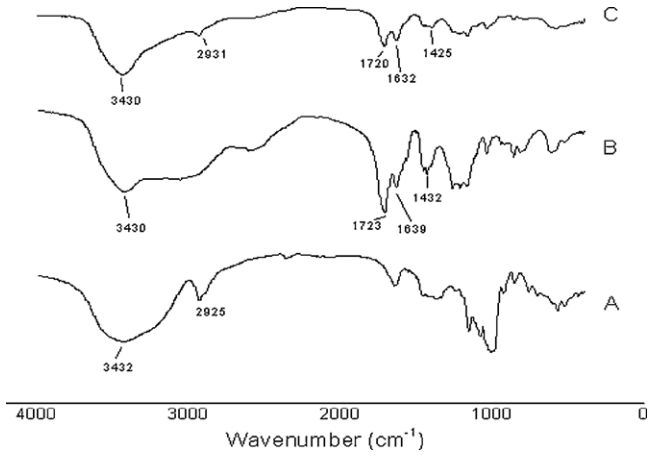

Fig. 1. The FTIR spectra of polysucrose (A), PAA (B) and polysucrose-based nanoparticles(C) (S2) are shown in the figure. It was observed that a large number of hydroxyl groups participated in the reaction.

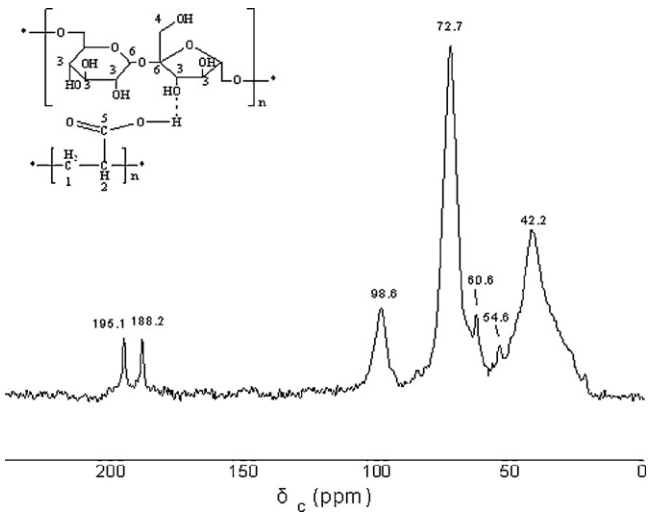

Fig. 2. The ^{13}C NMR spectrum of polysucrose-based nanoparticles is shown in the figure.

3. Results and discussion

3.1. Characterization of PS-based nanoparticles

3.1.1. Fourier transform infrared spectroscopy

The FTIR spectra of PS (A), PAA (B) and S2 PS-based nanoparticles(C) are shown in Fig. 1. The peak at 3432 cm^{-1} in spectrum (A), assigned to hydroxyl groups on the PS chain, was broad because of the hydrogen bonds association. The peak at 2925 cm^{-1} for PS (A) is assigned to the methylene stretching vibration. The peak at 3430 cm^{-1}, related to O—H in PAA in spectrum (B), is wider than the peak for PS. This is because PAA was easy to absorb water and then formed a lot of hydrogen bonds. Because of the effect of hydrogen bonds, the peak of hydrogen bonds had a red shift to 3000. The peaks at 1723 cm^{-1}, 1639 cm^{-1} and 1432 cm^{-1} of spectrum (B) proved the existence of COO^- groups. The peak at 2931 cm^{-1} in spectrum (C) represents the methylene stretching vibration in the complex. The peaks at 1720 cm^{-1}, 1632 cm^{-1} and 1425 cm^{-1} prove the existence of PAA in the product particles.

3.1.2. ^{13}C NMR analysis

The ^{13}C NMR spectrum of PS-based nanoparticles is shown in Fig. 2. The chemical shift of C-1 on the main chain of PAA is at 42.2 ppm. The chemical shift of C-2 is at 54.6 ppm, which indicates that the demagnetization shielding effect was enhanced. It is because of the α substituent effect of the carboxyl groups. The chemical shift of C-5 in O=C of the carboxyl groups is at 188.2 ppm. The chemical shift of C-4 joined to a primary hydroxyl group on PS is at 60.6 ppm. The chemical shift of C-3 joined to a secondary hydroxyl group is at 72.7 ppm. As it is affected by the electrophilic effect of the neighboring oxygen atom, the chemical shift of C-6, which is an anomeric carbon atom on the sucrose unit, is at 98.6 ppm. Because the content of MBA was small and the structure of MBA is similar with the structure of PAA, it is hard to identify the specific structure of MBA in the ^{13}C NMR spectrum. However, at 195.1 ppm is the peak of the carbon atom in the carbonyl groups in an amide group and it is clear. It shows the existence of the crosslinking agent.

3.1.3. Transmission electron microscopy (TEM) analysis

A TEM image of the S2 product nanoparticles is shown in Fig. 3. From this image, the product particles were found to be slightly ellipsoidal particles with good monodispersity and with diameter from 150 nm to 200 nm. Hydrogel is normally formed (Kang & James, 2007) when the bifunctional monomer MBA participates in the polymerization of acrylic acid, but the images show that when added to PS they formed nanoparticles, not hydrogel.

3.2. Influence of the reactant content on particle size and size distribution of PS-based nanoparticles

In this experiment, the PS content (50 ml of 50 g/l PS solution) was kept constant, the nanoparticles being obtained by altering the amounts of AA monomer, initiator CAN and crosslinker MBA.

3.2.1. Influence of the content of acrylate monomer on particle size and size distribution of nanoparticles

The average diameter and polydispersity index (PDI) of nanoparticles prepared from different R_{SM} ratio are shown in Fig. 4. The average diameter of nanoparticles became smaller with increasing R_{SM} (i.e. the decrease of AA content) when the R_{MI} and R_{MC} were kept constant. The results indicated that reducing AA content resulted in smaller nanoparticles. The reason is that increasing R_{SM} means decreasing the average length of PAA chains between cross-links, while the number of grafted chains of PAA and its crosslink density remained invariant. This will decrease

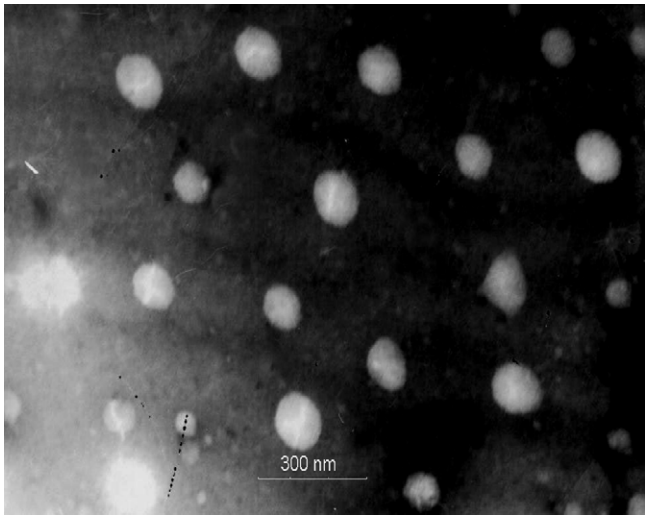

Fig. 3. The TEM image of the product nanoparticles is shown in the figure. From this image, the product particles were found to be ellipsoidal particles with good monodispersity and with diameter from 150 nm to 200 nm.

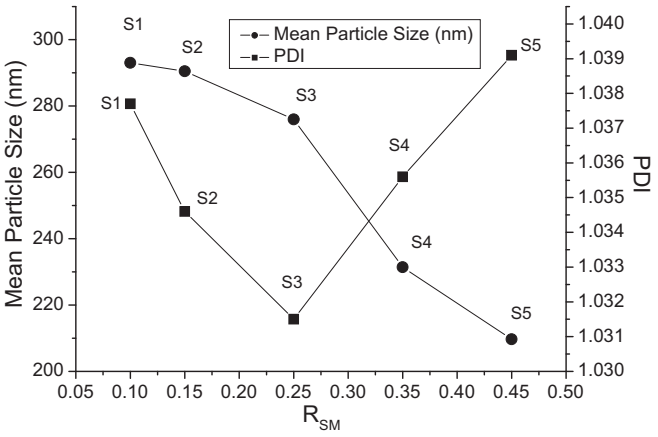

Fig. 4. The average diameter and polydispersity index (PDI) of nanoparticles prepared from different R_{SM} ratio are shown in the figure. The results indicated that reducing AA content resulted in smaller nanoparticles. If the AA monomer content was insufficient, some nuclei for growth could not obtain enough monomers, that is the monomers were unable to be assigned equally to each growth nucleus, which resulted in producing some smaller particles, and then a large PDI would be obtained.

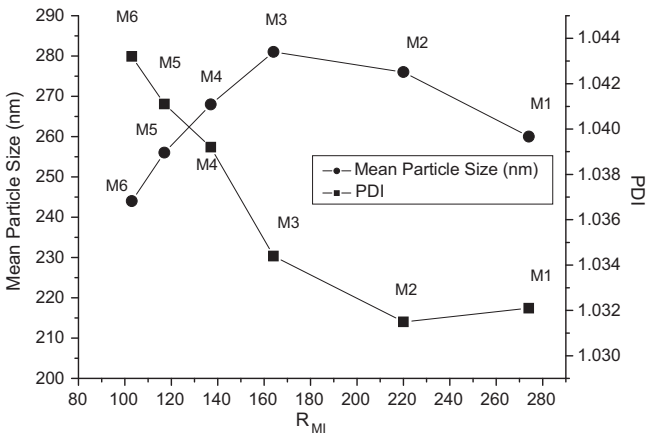

Fig. 5. The average diameter and polydispersity index (PDI) of nanoparticles prepared with different R_{MI} ratio (R_{SM} = 0.25 and R_{MC} = 35). With the increase of CAN content in the initial polymeric reaction stage, the concentration of free radicals on the macromolecular chains of polysucrose would increase in a unit volume (equal to the increase of concentration of polysucrose–AA complex).

the dimension of the PS–PAA complex, thus reducing the diameter of the nanoparticles. The value of polydispersity index (PDI) for all samples was relatively low indicating good monodispersity of the PS-based nanoparticles. The decrease of R_{SM} resulted in a decrease of the polydispersity index (PDI), for AA content up to R_{SM} = 0.25, followed by PDI increasing with the further decrease of R_{SM}. This may be because the dimensions of the PS–PAA complex were small in the initial reaction stage. These particles would play the role of the nuclei for growth, their dimension would become larger because of the extension and entanglement of PAA chains with the reaction continuing, and at last PS-based solid particles of dimensions in the nanometer range formed. If the AA monomer content was insufficient, some nuclei for growth could not obtain enough monomers, i.e. the monomers were unable to be assigned equally to each growth nucleus, which resulted in producing some smaller particles, and then a large PDI would be obtained.

3.2.2. *Influence of initiator content on particle size and size distribution of nanoparticles*

Fig. 5 shows the average diameter and polydispersity index (PDI) of nanoparticles prepared with different R_{MI} ratio (R_{SM} = 0.25 and R_{MC} = 35). There is a slight increase below R_{MI} = 164 and then there is a slight decrease for increasing R_{MI} (i.e. the decrease of CAN content), when the R_{SM} and R_{MC} were kept constant. With the increase of CAN content in the initial polymeric reaction stage, the concentration of free radicals on the macromolecular chains of PS would increase in a unit volume (equal to the increase of concentration of PS–AA complex). These complexes entangled with each other with the reaction going on, hence larger complexes were formed and cured to further form nanoparticles.

When excess CAN was added to the system, the concentration of free Ce^{4+} was maximized. The free Ce^{4+} cannot trigger free radicals on the PS chain, but they can induce chain transfer and chain termination, which reduced the degree of polymerization of the PAA and the dimensions of the complex were smaller (i.e. the dimension of nanoparticles were smaller).

With the increase of initiator CAN content, the distribution of particle size would broaden at the beginning of the reaction. With the initiator content increasing up to a certain value of R_{MI} (164), the distribution of particle size increased greatly. Although the increase of initiator content resulted in forming many active PAA side chains on the PS main chain in the initial reaction stage, the macromolecular chains of PS limited the diffusion motion of the active PAA side chains and had stabilizing function on the PS–PAA complex. In addition, as the concentration of AA monomer remained unchanged (R_{SM} = 0.25 and R_{MC} = 35), the increase of initiator had no significant influence on the distribution of particle size. When the concentration of AA reached more than a certain value (R_{MI} = 164), the Ce^{4+} chelating with PS was saturated. The free Ce^{4+} cannot trigger free radicals, but they were able to induce chain transfer and chain termination, which caused a lower degree of polymerization of some of the PAA side chains and smaller dimension of the complex, thus increasing the distribution of particle size slightly.

3.2.3. *Influence of crosslinker amount on particle size and size distribution of nanoparticles*

The average diameter and polydispersity index (PDI) of nanoparticles prepared with different R_{MC} ratio (R_{MI} = 220 and R_{SM} = 0.25) are shown in Fig. 6. The R_{MC} had a negligible effect on product particle size, when R_{SM} and R_{MI} were kept invariant. As the active free radicals were always located on the macromolecular chains of PS in the polymerization system, the PS of large molecular weight confined the movement of the free radicals, and the hydrogen bonds limited the movement of the grafted chains as well, both of which caused the conformational entropy of the active chain to be further reduced. Once a crosslinker molecule, which could make the growth nuclei particles merge with each other, diffused into the inside of a growing particles nucleus, it would be difficult to diffuse back to the surface, and thus reduced the possibility of causing merger and the particle size increasing. Therefore, the amount of crosslinker had an essentially negligible effect on particle size.

With the decreasing of R_{MC} (i.e. the increase of MBA content), the polydispersity of the particles increased slowly. Because the active polymer complex was driven to transform into a heterogeneous phase by hydrogen bonds in the system, the addition of crosslinker made these particles become unstable and increased the chance of crosslinking between particles, as a result, the number of large size particles increased in system.

As the polymer particles crosslinked and cured, the speed of monomer diffusing into the particle slowed down, which resulted in low efficiency. As the reaction continued, secondary nucleation on new PS molecules was generated and some new, small particles formed. When R_{MC} < 35, both of these facts induced the

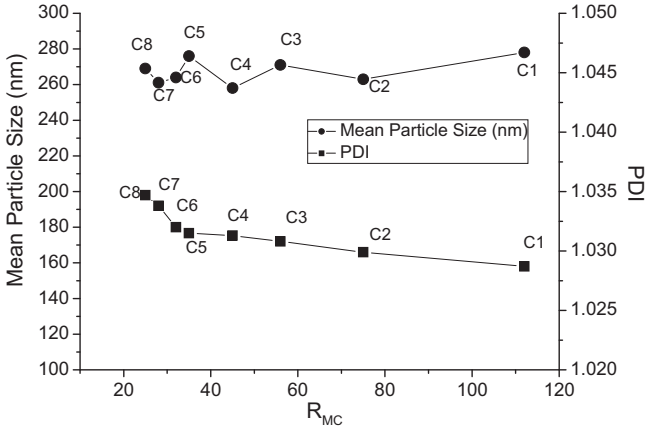

Fig. 6. The average diameter and polydispersity index (PDI) of nanoparticles prepared from different R_{MC} ratio (R_{MI} = 220 and R_{SM} = 0.25) are shown in the figure. As the active free radicals were always located on the macromolecular chains of polysucrose in the polymerization system, the polysucrose of large molecular weight confined the movement of free radicals, and the hydrogen bonds limited the movement of the grafting chains as well, both of which induced the conformational entropy of the active chain to be further reduced.

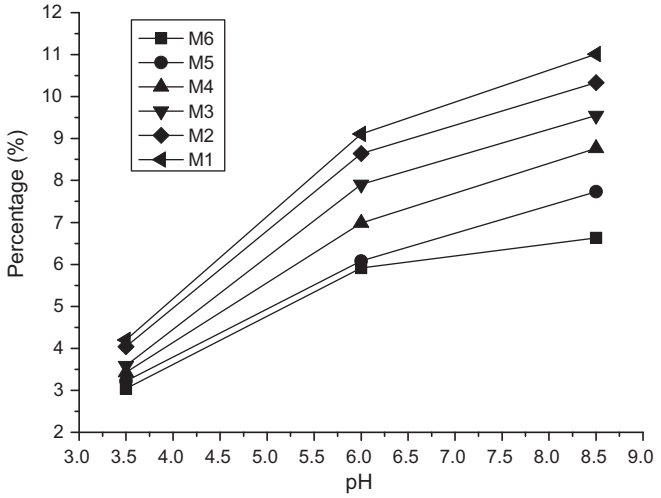

Fig. 8. The AE of the nanoparticles at different pH value. It show that the protein AE of nanoparticles was low when the pH was 3.5, but the BSA adsorbing efficiency of the nanoparticles was significantly enhanced as the pH value was increased. This was ascribed to the enhancement of alkalinity in the system.

polydispersity of PS-based nanoparticles to increase with the increasing of crosslinker content.

3.3. Adsorbtion efficiency analysis

3.3.1. Influence of AA content on BSA adsorbing efficiency of PS-based nanoparticles

Fig. 7 shows the absorption efficiency (AE) of nanoparticles prepared from different R_{SM} ratio at fixed R_{MI} and R_{MC} (R_{MI} = 220 and R_{MC} = 35). The BSA AE of the nanoparticles increased with the decrease of R_{SM} (i.e. the increase of AA content). All added AA was grafted on the PS chain, which ensured that there was no excess AA monomer in the system. The increase of AA content resulted in an increase of carboxyl content in the product particles, which enhanced the electrostatic interaction between product particles and BSA, so that the protein AE increased. Therefore, to improve the AE of the product particles, one should increase their carboxyl content.

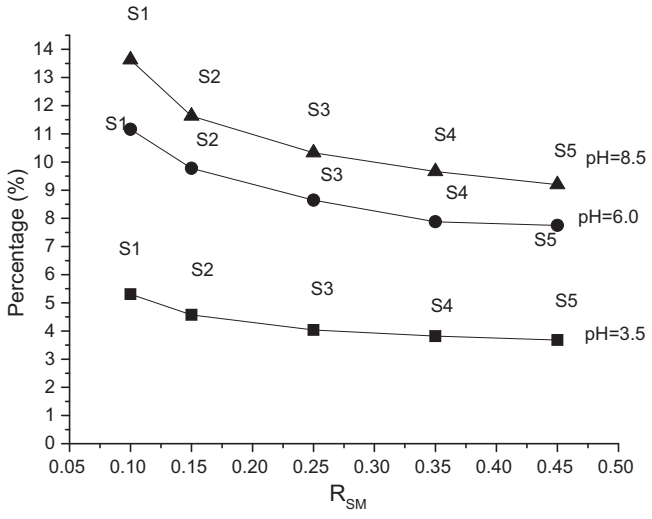

Fig. 7. The absorption efficiency (AE) of nanoparticles prepared from different R_{SM} ratio at fixed R_{MI} and R_{MC} (R_{MI} = 220 and R_{MC} = 35). The increase of AA content resulted in an increase of carboxyl content in the product particles, which enhanced the electrostatic interaction between product particles and BSA, so that the protein AE increased. Therefore, to improve the AE of the product particles, one should increase their carboxyl content.

3.3.2. Influence of pH value on adsorbing efficiency of nanoparticles

Fig. 8 shows the AE of the nanoparticles at different pH value. It show that the BSA AE of nanoparticles was low when the pH was 3.5, but the BSA adsorbing efficiency of the nanoparticles was significantly enhanced as the pH value was increased. This was ascribed to the enhancement of alkalinity in the system. The —COOH contained in the nanoparticles ionized gradually, producing —COO^- with negative charge, which enhanced the charge density on the nanoparticles surfaces and reinforced the electrostatic interaction between nanoparticles and BSA, hence, increased AE.

When the system pH value was increased from 6.0 to 8.5, the BSA AE of the nanoparticles continued to improve, but at a lower rate. On one hand this was due to the strengthening of the alkalinity in the system with the —COOH contained in the nanoparticles being ionized totally. The COO^- with negative charge aggregated on the hydrophilic surface of the nanoparticles and resulted in enhancing the protein AE of the nanoparticles. On the other hand, the surface electric potential of the BSA changed from positive to negative in the alkaline environment. This change offset the electrostatic interaction between some nanoparticles and BSA, and induced the decrease of the rate of increase of the AE of the nanoparticles of the samples M1–M6 showed that the protein AE of the product particles increased from M1 to M6 gradually as the pH value increased. The reason is that when R_{MI} increased, the added amount of initiator CAN decreased, which resulted in a decrease of active sites on the macromolecular chains of PS. When the added amount of AA was kept constant, but the initiator CAN decreased, the increase of the PAA-graft-chain length induced part of the PAA-graft-chains to protrude from the surface of the nanoparticles. The more the added amount of initiator CAN, the shorter the length of extending of PAA-graft-chain would be. Due to in the absence of shielding effect by the PS chain segments, the PAA chain segments, which have already extended from the particle surface, absorbed BSA more easily than the PAA chain segments on particles surface, so the AE of the particles increased.

4. Conclusions

With the PS content kept constant, nanoparticles were obtained by altering the amounts of AA monomer, initiator CAN and crosslinker MBA. The influence of the ratios of reactants on particle size and size distribution of PS-based nanoparticles and the protein AE of nanoparticles under different pH value were investigated. FTIR, ^{13}C NMR and SEM were utilized to characterize the structure and morphology of the PS-based nanoparticles. The results indicated that the average dimension of the nanoparticles increased from 210 nm to 293 nm and the PDI varied from 1.04 to 1.03, with the increase of AA content (from 1.2 g to 5.3 g), while the R_{MI} and R_{SM} were kept constant. The average dimension of the nanoparticles varied from 244 nm to 281 nm, and PDI increased from 1.037 to 1.04, with the increase of initiator content (from 0.06 g to 0.16 g), at the fixed R_{SM} and R_{MC}. To a certain extent, the addition amount of crosslinker CAN had negligible effect on the system. The protein adsorption efficiency of the nanoparticles increased from 5.3% to 13.6%, with the increase of solution pH value (from 3.5 to 8.5).

This kind of PS-based nanoparticles not only has good biocompatibility, low toxicity and good hydrophilicity of polysaccharide-based media, but also have controllability, so it is of great application value. This study extends the application of natural sugar, as well as opens up a broad development potential for the sugar industry.

References

Birringer, R., Gleiter, H., Klein, H. P., & Marquardt, P. (1984). Nanocrystalline materials an approach to a novel solid structure with gas-like disorder. *Physics Letters A*, *8*(102), 365–369.

Donald, W. A., Annette, P., & Thomas, G. P. (1975). Separation of epithelial cells from suspensions of cells from the hamster parotid gland in an isokinetic density gradient of Ficoll in tissue culture medium. *Analytical Biochemistry*, *66*, 353–364.

Fischer, F. D., Waitz, T., Vollath, D., & Simha, N. K. (2008). On the role of surface energy and surface stress in phase-transforming nanoparticles. *Progress in Materials Science*, *3*(53), 481–527.

Gregory, L., Elias, F., & Patrick, C. (2001). Nanoparticulate systems for the delivery of antisense oligonucleotides. *Advanced Drug Delivery Reviews*, *47*, 99–112.

Hari, S. S., & Aruna, S. (2007). Nanoparticles aggravate heat stress induced cognitive deficits, blood–brain barrier disruption, edema formation and brain pathology. *Neurobiology of Hyperthermia*, *162*, 245–273.

Jae, G. R., Young, J., In, S. K., Jong, H. L., Jae, W. N., & Sung, H. K. (2000). Clonazepam release from core–shell type nanoparticles of poly(ε-caprolactone) /poly(ethylene glycol)/poly(ε-caprolactone) triblock copolymers. *International Journal of Pharmaceutics*, *200*, 231–242.

Kang, H., & James, M. D. (2007). Development and characterization of poly(vinylidene fluoride)–poly (acrylic acid) pore-filled pH-sensitive membranes. *Journal of Membrane Science., 1–2*(301), 19–28.

Peter, N. L., Olgal, I. M., & Olga, V. O. (1987). On the separation ability of various Ficoll gradient solutions in zonal centrifugation. *Analytical Biochemistry*, *166*, 287–297.

Rodrigues, J. S., Santos-Magalhaes, N. S., Coelho, L. C., Couvreur, P., Ponchel, G., & Gref, R. (2003). Novel core(polyester)–shell(polysaccharide) nanoparticles: Protein loading and surface modification with lectins. *Journal of Controlled Release*, *92*, 103–112.

Richard, H., Andreas, M. W., & Wolfgang, V. (1986). Usefulness of Ficoll in electric field-mediated cell fusion. *Life Sciences*, *39*, 2279–2288.

Suphiya, P., & Sanjeeb, K. S. (2008). Polymeric nanoparticles for cancer therapy. *Journal of Drug Targeting*, *2*(16), 108–123.